



# Magnetically impelled arc butt welding (MIAB): a comprehensive review on welding parameters, microstructure, and joint performance

S. Santhosh Kumar<sup>1</sup> · S. Ramesh Kumar<sup>1</sup>

Received: 3 August 2023 / Accepted: 22 September 2023 / Published online: 4 October 2023  
© International Institute of Welding 2023

## Abstract

Magnetically impelled arc butt welding (MIAB) is a solid-state pressure welding technique used to join tubes and pipes, which does not require edge preparation and filler material. Heating the material on both the tube surface ends by producing a rotating arc using an electromagnetic force improves the arc rotation. Applying the forging pressure on the movable end of the tube will join with the other end surface of the tube. Unlike conventional welding, the weld formation is developed with a single-step process without several passes. The parameters such as welding current, exciting coil current, coil position, and gap size between the tubes influence the weld strength. This review focuses on MIAB welding stages with process parameters and MIAB welded of similar and dissimilar materials, including the microstructure of weld and joint performance and the process parameters that affect the property of welded materials and researcher inferences; applications were discussed.

**Keywords** MIAB · Arc rotation · Electromagnetic force · Dissimilar welding · Microstructure

## 1 Introduction

Magnetically impelled arc butt (MIAB) welding is a unique method of joining tubes using electromagnets or permanent magnets interacting with electric current. It forms an electromagnetic force (EMF or F), which creates an arc along the pipe circumference. The components are forged after a specific heating period to form a weld [1, 2]. E.O. Paton Electric Welding Institute initially explored this process during the 1950s and 1960s [3, 4]. This welding method is primarily adopted in European countries for automotive components of tubular parts with pipe thicknesses ranging from 0.6 to 16 mm (thick-walled tubes). Figure 1 shows the stages in the MIAB welding. The main components of the MIAB welding are tube material, power source, electromagnets or permanent magnets, hydraulic power pack, and control unit. In the MIAB welding setup, one tube is fixed, and the other tube is movable. Both tubes are not rotating; instead, they move

in linear motion. Selecting a magnet or electromagnetic coil and maintaining a minimum distance from tube ends are essential for MIAB welding. There are four steps in the tube joining process, from arc initiation until forging. The four stages of MIAB welding are arc initiation, beginning of arc rotation, arc stabilization, and upsetting [5].

Stage 1: The first stage is the arc initiation process, where the magnetic coil arrangement is kept on the tubes, which allows the current flow through the tubes.

Stage 2: The materials must keep a minimum-defined gap for creating an arc. The air gap between the tube material is maintained at a minimum gap distance of 1.5 to 2 mm. The welding current and magnetic coil switch produce an EMF between the tube faying surfaces. The arc formation is generated on the interior surfaces of tube material.

Stage 3: The sustained arc starts rotating with a magnetic coil current between the tubes in the arc rotation stage. The electric arc slowly generates and attempts to get out from the tube inner edges to the outer ends. It depends primarily on the coil position, gap size, and coil excitation. The stabilized electric arc gets a continuous uniform ring due to high rotating velocity, which heats the tube surfaces and produces a thin molten layer.

Stage 4: The final stage is the upsetting stage, where the development of molten metal structures in the arc gap leads to high arc velocity variations to cause arc rotation

---

Recommended for publication by Commission III - Resistance Welding, Solid State Welding, and Allied Joining Process

✉ S. Ramesh Kumar  
srk1306@gmail.com

<sup>1</sup> School of Mechanical Engineering, SASTRA Deemed to be University, Thanjavur, Tamilnadu 613401, India

instability. The increased current supply in milliseconds generated in tube material forms a red-hot condition where bridge formation occurs to perform the forging operation. Then, the forging process takes place by applying pressure on the movable tube material to join the molten tube edges.

The welding current is split into three stages, and the duration is divided into four stages. Tables 1 and 2 demonstrate their corresponding actions for the ferritic steel T11 material with an OD of 48 to 54 mm and a wall thickness of 6 to 7 mm [6, 7]. The duration and amperage requirements for the various stages of MIAB welding are governed by the process and the material being welded. Using the material's properties, it can predict the energy needed to heat it to its solidus temperature. Compared to other solid-state welding methods, the time taken for this type of weld is considerably shorter. Limited exploration has been conducted on extending the implementation of the MIAB welding process to non-ferrous materials, as its focus is primarily on ferrous materials.

Fleming's left-hand rule principle defines arc rotation perpendicular to the welding current and the magnetic field. It is the same as the principle of the arc displacement process shown in Figure 2 [8].

The axial welding current ( $I_a$ ) and radial magnetic flux density ( $B_r$ ) induce a force which causes arc displacement and pushes it towards the exterior edges of the tubes. The Lorentz forces determine the EMF in the external magnetic field that interacts with the electron on the arc. The EMF is obtained from Eq. (1):

$$F = KI_a \times B_r \tag{1}$$

where K is the coefficient, which depends on the tube gap size. The force applied to the welding current is proportionate to the arc rotation in MIAB welding.

One of the notable advantages of MIAB welding is its solid-state process, which results in a shorter weld cycle, reduced energy input requirements, absence of component rotation, and minimized material loss. MIAB welding is

**Fig. 1** Schematic diagram of stages in the MIAB welding **a** Stage 1, **b** Stage 2, **c** Stage 3, and **d** Stage 4 [5]

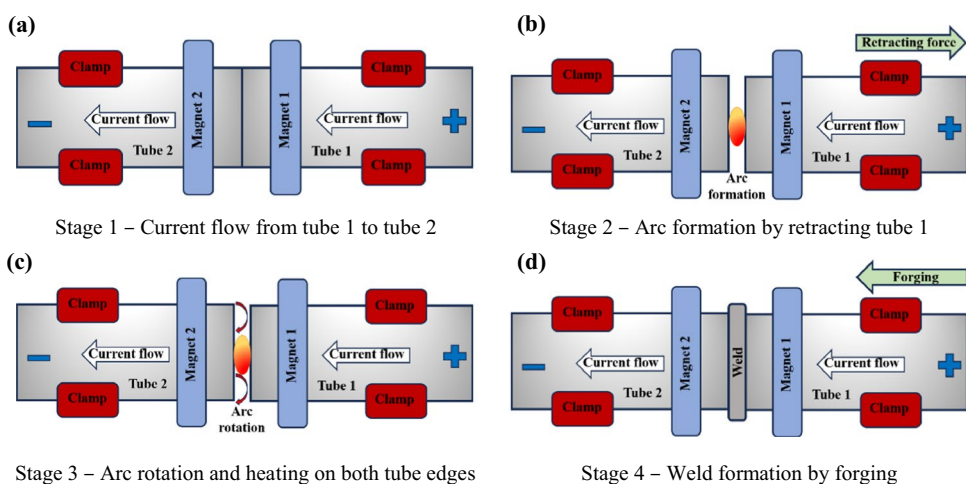


**Table 1** Welding current stages in the MIAB welding for T11 [6, 7]

S. no.	Current	Action performed	Current ranges (A)	References
(1)	Arc initiation current (I1)	Tube pressing and initiation of the arc	280–300	[6, 7]
(2)	Arc rotation current (I2)	Stable arc rotation and heating of tubes	200–220	
(3)	Upset current (I3)	Tube upsetting	1100	

**Table 2** Welding time stages in the MIAB welding for T11 [6, 7]

S. no.	Welding time	Action performed	Time ranges (s)	References
(1)	Tube pressing time (T1)	Tube pressing	0.5–1	[6, 7]
(2)	Arc initiation time (T2)	Initiation of arc and keeps rotating	4–6	
(3)	Arc rotation time (T3)	Formation of stable arc and heats the tube edges	20–30	
(4)	Upset time (T4)	Tube upsetting	0.3	

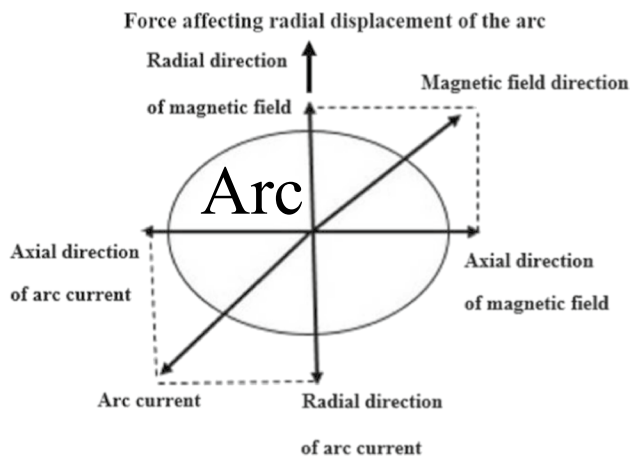


**Fig. 2** Arc displacement process in MIAB welding [8]

differentiated from other solid-state welding processes by its low cost, superior control, and reliability. This method is unique because it may create strong welds without surface preparation or with the weld tubes positioned with an axial offset. However, there are some restrictions on its use with tubes thicker than 6 mm, which prevents its wide adoption in the industrial sector. As a result, more studies have examined the viability of employing MIAB welding on thicker tubes using conventional setups. To achieve successful MIAB welds, certain conditions must be met, namely:

(a) On the two weld surfaces, the active locations of the rotating arc should nearly match the thickness of the weld.

(b) Less than 0.7 mm of non-uniformity should be maintained on the faying surfaces [5].

The controlled conditions of the rotating arc depend on the welding current, exciting coil current, coil position, and gap size between the tubes. The rotation of the arc and its position within the tube gap size depend on the strength of the magnetic field and the welding current. The distance between the tubes and the position of the magnet both affect the distribution of the magnetic field. Heat is created on the outside surface of the weld metal while the arc rotates, which is subsequently dissipated by convection and radiation. The weld quality can be negatively affected by uneven heat generation brought on by the arc's movement from the inner to the outer diameter of the tube gap.

According to Taneko et al., when MIAB welding of steel pipes, arc rotation velocity fluctuates over time and is separated into three regions: low rotation velocity, high rotation velocity, and the rotation velocity fluctuation region. The author conducted experiments using various input current and magnetic coil current in different areas of the tube. They noticed that the arc rotational velocity increased by 8 to 10 m/s from the low-velocity to the high-velocity region. This causes the arc to accelerate from the high-velocity zone to the region of rotational velocity variation at a speed of 50 to 55 m/s [9]. Also,

Sato et al. studied the arc rotation movement of the steel pipe from the inner to outer edges of the tube end. They noticed that the magnetic blow effect causes the arc to move toward the inner diameter when initiated. This phenomenon is brought on by the creation of a high-gradient external magnetic field as a result of the interaction between the natural magnetic field of the arc and the geometry of the tube [10]. Iordachescu et al. investigated the longitudinal magnetization method to satisfy the magnetic flux density. The authors further stated that arc rotation and heating time are essential in delivering successful weld joints, and also, high-quality welded joints are made by controlling the arc displacement [11]. Kuchuk-Yatsenko et al. controlled the radial arc displacement by changing the strength and direction of the magnetic field. The strong magnetic field surrounding the outer diameter pulls the arc towards the direction of the inner diameter. As a result, uniform heating at the joint is ensured by the rotating arc and thermal conductivity of the welded metal. Controlling the arc displacement created the uniform weld joint [12]. Kim et al. proposed a 2D finite element model to evaluate the magnetizing force distribution. The higher magnetic field strength induces uniform heating through the increased force on the arc and arc speed rotation. It can be concluded that maximum flux density is needed to attain better weld quality. This can be achieved by increasing the coil current and decreasing the gap between the tubes and coil position [13]. So, the magnetic flux density depends on the coil position, coil current, and gap size between the tubes or pipes.

Vendan et al. confirmed this by conducting a MIAB welding trial on high-pressure tubes (SA210 A-1). They worked an experiment trial by adjusting the process parameters on both weld tubes, performed a bend test, and obtained no open discontinuity on both tube materials [14]. MIAB welding has been the main technique for combining ferrous tubes to produce various components in the European automobile sector. The power sector has also looked at MIAB welding to produce boiler tubes, heat exchangers, and other high-pressure components used in hazardous and corrosive conditions. Balta et al. confirmed this by FE analysis of the fender bracket, and results are compared with the experiment. It showed no failure in the MIAB-welded fender bracket and that MIAB-welded components are appropriate for vibration-induced parts [15]. Systematically, this review gives a comprehensive overview of the MIAB welding process parameters and their effects, as well as the attributes of weld quality, material combinations, and industrial applications associated with MIAB welding.

## 2 Parameters influencing weld quality in MIAB weld

The MIAB welding process greatly depends on the input process parameters. The process parameters such as welding current, coil position, coil current, and gap size between the tubes influenced the weld strength. Variations in the welding current and time duration make the joints irregular if the current is too high. Also, the tube thickness and the choice of material determine the range of operating parameters. Panda et al. investigated the arc speed of T11 steel tubes through experimental and numerical studies. Input factors, including welding voltage, magnetic coil voltage, welding current, and magnetic current, are considered while evaluating it using Multi-gene genetic programming (MGGP). According to the MGGP results, Figure 3 shows that the welding current controls the arc speed more than the other factors [16]. In MIAB welding, welding current is classified into three stages based on welding time duration in each stage: arc initiation current, arc rotation current, and upset current. The effects of process parameters in MIAB welding are stated below.

### 2.1 Effect of arc initiation current

The arc initiation current delivers sufficient heat to the tubes or pipes and interacts with the magnetic field producing a rotating arc. The electric arc creates a uniform heat distribution through the magnetizing coil on the tubes. Changes in arc speed can also generate non-uniform heating, which can be solved by modifying the magnetic field distribution [17]. The amount of electric current flowing from the power source point to the arc is inversely proportional to the distance between them. The electric current in front of the arc

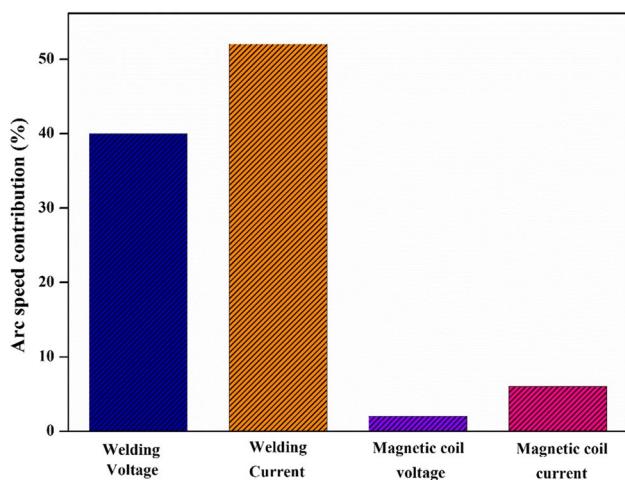


**Fig. 3** Percentage contribution of different inputs to arc speed in the MIAB welding [16]

rises as it approaches the power supply point, while the current behind it drops [9]. The arc movement is increased by increasing the magnetic coil current and welding current, which produces heat to the faying surfaces of both tubes. Vendan et al. stated that the ferritic material of T11 crosses the curie temperature (770 °C), which becomes paramagnetic and pushes the arc toward the exterior edges of the tube surface [18]. This can be confirmed by the arc movement relation by the gap between the tubes and the welding current with the magnetization current range of 0.3 to 0.7 A, shown in Figure 4 [11]. In the area I region, the arc rotates unpredictably for higher current but does not move at all for low currents. The distance between the tubes cannot generate an acceptable magnetic force value, even with sufficient welding current and magnetic fields. The stability of the arc formation is discussed in area II, which rotates between the tube interface. Due to an enormous gap value of the distance between the tubes and inadequate current, the arc in area III starts but ends quickly, i.e., it does not start rotating, or its rotation is unstable. If the upsetting occurs during unstable welding, the joint either does not form or has insufficient strength (areas I or III). Vendan et al. experimented with MIAB-welded T11 alloy steel joints for boilers and found that the insufficient weld current at reduced gap distance causes shorting of tubes [6].

### 2.2 Effect of arc rotation current

The arc rotation effectively regulates the heating of tube edges, which changes the microstructure and the weld interface. It occurs primarily due to the strong magnetic field

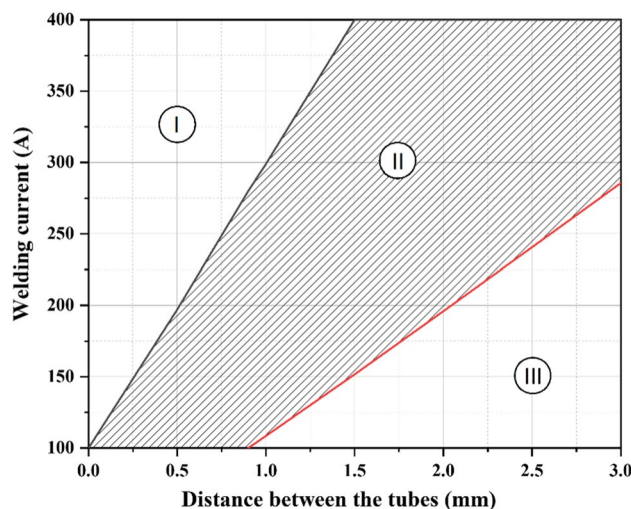


**Fig. 4** Relation between the welding current intensity (A) versus distance between the tubes (mm): area I—with unstable rotation or without arc movement; area II—proper arc initiation and stable rotation; area III—short lifetime arc with an unstable rotation or no movement [11]

carried by an electric current around the tube circumference, and the amount of arc rotation current depends on the pipe wall thickness and the induced current on the coil. Due to the thin wall of the pipe, the arc rotates at high speed, and the magnetic flux density also increases at the initial level. This flux density can be measured by using a Gaussmeter. It has been confirmed that the flux density increases with arc rotation increase [10]. So, the arc rotation is influenced mainly by magnetic flux density. In terms of evaluating the weld quality, the arc rotation current is the most significant factor. For the tube-to-tenon joint of mild steel, a better weld is attained at the higher welding current of 250 A for 10 s and an upset current of 400 A for 1 s at a 2-mm air gap, 50 V arc voltage, and 3000 gauss magnetic field [19]. The type of material used determines the time duration and amperage requirements in MIAB welding.

Figure 5 depicts the graphical comparison of the ultimate tensile strength (UTS) of MIAB-welded T11 tubes with arc rotation time (T3), demonstrating that the UTS is higher when T3 is 20 s. The UTS value is moderately lower for T3 above or below 20 s. Figure 6 explains the current inputs, such as I2 and I3 vs UTS. It demonstrates that the upset current increases, diffusion increases, leading to increased penetration depth and tensile strength. Therefore, the increment in arc rotation current and upset current enhances the tensile strength of the T11 tubes. Previous studies on MIAB-welded carbon steel tubes have shown that a lower arc rotation current leads to incomplete expulsion of the decarburized zone, forming a light band zone with a more ferritic structure along the weld line. This can be eliminated by a higher upset current and showed better tensile properties at the weld interface [20]. It has been demonstrated that the upset current impacts expulsion during the upset stage. In contrast, the arc rotation current is responsible for heating the weld surfaces to the solidus temperature, which causes

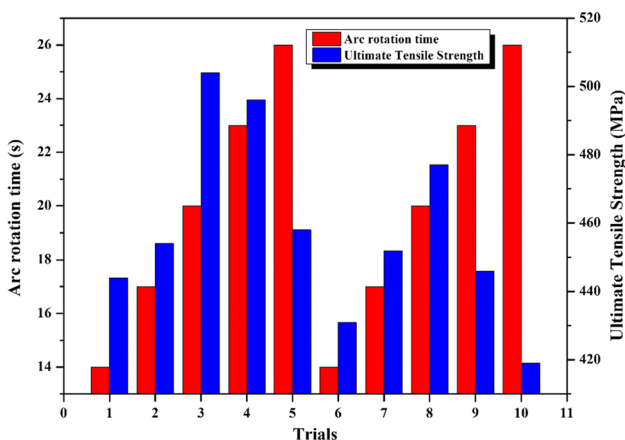


Fig. 5 Graphical comparison of the ultimate tensile strength (UTS) of MIAB-welded T11 tubes for arc rotation time (T3) [7]

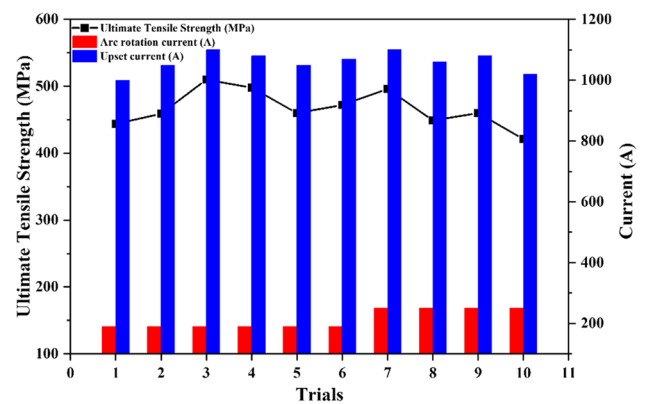


Fig. 6 Graphical comparison of the ultimate tensile strength (UTS) of MIAB-welded T11 tubes according to arc rotation current (I2) and upset current (I3) [7]

the material to plasticize. In MIAB welding, welding time and current impact penetration depth depend on the welding geometry and material properties.

### 2.3 Effect of upset current on weld

The short pulse of high current applied before to upset is known as upset current. It is crucial to remove contaminants and molten metal from the weld interface. The microstructure depends on lower or higher upset current. The upset current determines the width of the TMAZ region. The higher the upset current causes, the smaller width of the TMAZ region. A lower upset current produces low heat and an incomplete expulsion of molten metal. Excess surface metal expulsion from the weld interface can occur from the high upset current, forming voids. Sivasankari et al. experimented on carbon steel tubes (44 mm OD and 4.5 mm thickness) by varying the upset current over 800 A. This provided sufficient edge surface heating and significantly impacted the weld structure, as shown in Figure 7. During the tension test, fracture occurs in a weaker region where samples welded using a lower upset current displayed a noticeable decarburized zone. Consequently, the fracture happens at the weld due to its comparatively weaker microstructure.

In contrast, when samples are welded with a higher upset current, the weld interface is strengthened due to the formation of acicular ferrite. Acicular ferrite offers superior strength and toughness and is the favoured microstructure in the weld interface [21]. Dhivyasri et al. confirmed this on T11 tubes and observed that the lower upset current gets a small amount of heat on the tube and forms a low deformation at the upsetting phase, which resulted in weak weld formation [7]. Kumar et al. conducted dissimilar welding of T11 and T91 steel tubes with the upset current range of 900–1100 A, which provides good weld strength and homogenous microstructure [22]. The combination of

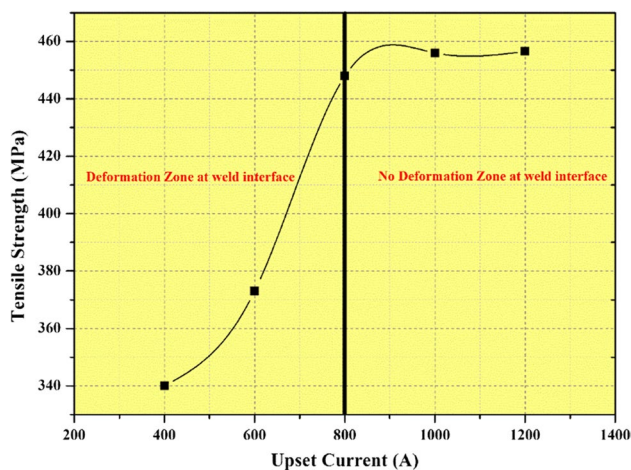


**Fig. 7** Effect of upset current (A) vs weld tensile strength (MPa) for MIAB-welded carbon steel tubes [21]

lower arc rotation current and high upset current causes the main void formation and poor weld. But Isravel et al. found that the lower upset current and lower arc rotation current deteriorate the UTS value in SA210 GrA tubes. That is relative to the number of voids with upset current interaction [23]. From this, it can infer that the material properties and geometry influence the welding current, time duration, and pressure values.

## 2.4 Effect of coil position

In MIAB welding with electric current aid, the magnetic field is obtained through several coils. The 1000–2000 amp-turn (At) magneto motive force produces a 0.02–0.1 T [8]. The EMF equation states that increasing the welding current and magnetic field results in a faster arc rotation. The small gap between coil distances explained an outstanding magnetic flux line distribution in the arc gap, i.e., induced magnetic flux lines are formed in the space between the coils. The magnetic flux distribution has been high at the gap between the pipes by placing an electromagnetic coil at a small gap-to-coil distance. Magnetic flux density has shown an increase as the coil distance difference increases. Norrish et al. developed a model for thin-walled transmission pipelines using Maxwell magnetic simulation software. The magnetic path configurations and the parameters confirmed that uniform arc heating developed before forging [24].

## 2.5 Effect of gap size

Kachinsky et al. explained that a stable arc formation depends on arc gap size and parallelism of tube ends. With the help of magnetic flux density, the gap size is the distance between the two tubes where the arc has been formed. The

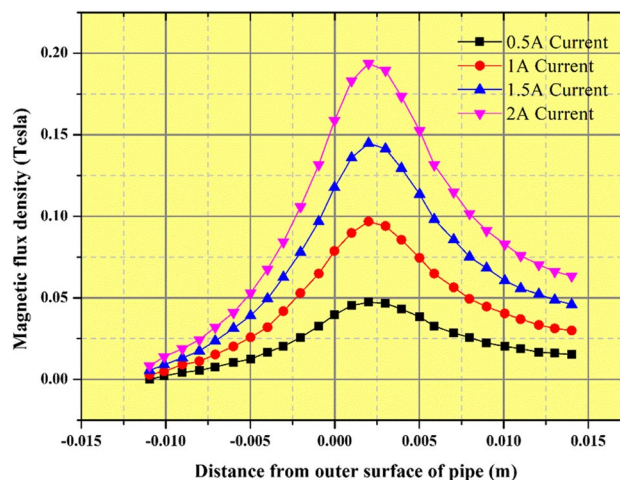


**Fig. 8** Graphical comparison of magnetic flux density (T) corresponding to exciting current (0.5 A, 1 A, 1.5 A, 2 A) in an outer surface of the pipe at various distances (m) [26]

gap size increases as the end face of the pipe melts off. The controlling magnetic field is present on the arc gap size, enhancing the arc movement and developing the quality of welded joints. The magnetic flux distribution is disturbed by the gap size, which determines the rotating arc behaviour—the tube gap size reduces and thus increases the flux density of the material [25].

The gap size usually is 1.5–2 mm, which increases the magnetic flux density and improves arc rotation. Although the distribution of magnetic flux is smaller when the distance exceeds 2 mm, the arc disappears. Figure 8 shows the graphical comparison of magnetic flux density (T) corresponding to exciting current (0.5 A, 1 A, 1.5 A, 2 A) in the outer surface of the pipe at various distances (m). The magnetic flux density values gradually rise when the distance between the pipes shifts from the outside surface of the pipe towards the middle [26].

## 2.6 Effect of exciting coil current

A 2D finite element model was developed by Kim et al. to study the magnetic flux density distribution of electromagnets in the MIAB weld joint. By examining the radial magnetic field between the two steel pipes, they could determine the relationship between the strength and quality of the weld joint. They also concluded that a stronger magnetic field causes the arc to experience a maximum force, which speeds up the arc and increases heating [13]. Vendan et al. analyzed the modelling of magnetic flux distribution in MIAB welding using finite element analysis. Using a three-dimensional finite element model, the relationship between magnetic flux density and the interdependence of MIAB welding parameters were demonstrated. These parameters include gap size,

exciting coil current, and coil position relative to the weld center. These parameters collectively govern the electromagnetic force generated during the welding. This simplifies designing an effective magnetic setup for MIAB welding [27]. So, the design of the electromagnet and the amount of exciting current used to determine the magnetic field distribution is more significant. Vendan et al. utilized a 2D and 3D FEM model to evaluate the magnetic flux distribution and electromagnetic force. They observed that the distribution of magnetic flux in the tube gap exhibited an inverse relationship with the distance of the tube gap and the position of the electromagnetic coil relative to the weld region. Additionally, they found that the magnetic flux distribution was directly proportional to the exciting coil current [3].

### 3 Properties of welded materials by MIAB welding technique

#### 3.1 Low-carbon steel

Low-carbon steels are iron-carbon alloys with a carbon concentration of 0.1 wt%. At eutectoid temperature, the carbon content is found in the single-phase  $\alpha$ -ferrite, a ferromagnetic phase with a BCC structure [28]. In low-carbon steel, spot and projection welds are attempted. The welding requires a high electrode force after the pulse current, and the weld joints need a tempering process [29, 30]. Gas tungsten arc welding (GTAW) and gas metal arc welding (GMAW) are the standard welding methods used to join low-carbon steel, but low efficiency and low quality are the preliminary problems [31]. The following applications have successfully used neodymium-doped yttrium aluminium garnet (Nd: YAG) and carbon dioxide (CO<sub>2</sub>) systems [32]. MIAB welding is the perfect method for joining low-carbon steel tubes, which shows the uniform bead and weld penetration in Figure 9 [6]. Researchers like Sivasankari et al. prepared the MIAB welding experimental setup and procedure for boiler-graded materials T11. The arc rotation speed and arc characteristics were discussed, and the microstructural analysis of several samples was carried out by varying the input parameters [21]. Nandakumar et al. made a half-factorial experimental design by changing arc stabilization time and upset current during MIAB welding of T11 tubes [33]. Vendan et al. experimented with non-destructive testing for MIAB-welded T11 joints, and the quality of the joints was within the acceptable limit [34].

#### 3.2 Medium carbon steel

Medium carbon steels are similar to low-carbon steels but contain more carbon and manganese, with concentrations of 0.3 to 0.5% and 0.6 to 1.65%, respectively. It is most



Fig. 9 Uniform bead and weld penetration of MIAB-welded T11 tubes [6]

necessary when higher mechanical properties are required for the products. Higher Mn, C, or both usually improve section thickness, mechanical properties, or hardening depth [35]. Medium-carbon steels may be tempered and quenched by raising the carbon content to around 0.5% and increasing the manganese content [36]. Mostly, these steels are in tempered conditions and have tempered microstructure. The continuous welding of medium carbon steels should be performed either with controlled hydrogen fillers or a low-hydrogen welding method. MIAB welding plays a significant role in production with a better quality of welds for higher productivity. During morphology inspection, MIAB-welded samples revealed excellent weld integrity [23].

#### 3.3 Aluminium alloys

Aluminium (Al) alloys occupy the highest quantity and application in non-ferrous metals. Since extensive research was carried out on the application, less knowledge of the phase composition and transformations was obtained during solidification, cooling, and heating [37]. The polymer-matrix composites used in Al alloy have commonly been adopted for aerospace structures [37–39]. Al alloys are considered for heat treatment procedures such as precipitation hardening, annealing, ageing at either room temperature or elevated temperature, and quenching. Welding of alloys is considered a challenge due to their high thermal conductivity and low hydrogen solubility, regardless of the welding method used. Laser welding provided some additional burden due to the reflective surface produced during the process [40].

For non-ferrous materials, MIAB welding is challenging to attain the magnetic flux density at the welded region. Mori et al. experimented with MIAB welding on aluminium

and copper joints. A ceramic shading bar was positioned between the pipes to measure the number of arc rotations. The electromagnetic oscillograph records the arc rotation as it passes through a specific section of the pipe circumference. The shorter distance between the coils ( $2L = 40$  mm) produces a magnetic flux distribution by increasing the exciting coil current. However, the arc rotation was insufficient because its non-magnetic material do not have uniform fusion. It can be accomplished by placing a ferromagnetic iron core on the pipes to enhance the magnetic flux density, resulting in uniform weld strength. Even the actual distance of the coil ( $2L = 230$  mm) with the iron core of Al produces a magnetic flux density nearly equal to that of steel pipes, as shown in Figure 10. Welding aluminium-copper (Al-Cu) joints effectively sets the Al on the negative side and the Cu on the positive side. Additionally, the negative side of Al produces arc penetrations on the inner area, and it rotates the arc more, which tends to heat the end face of pipe [41].

### 3.4 MIAB welding of dissimilar grade materials

Generally, in boiler header assembly, P91 is used as the header, and the pipe can be used from low-alloy steel such as P11 or P22 steel [42, 43]. These involve welding between these two distinct steel grades of Cr-Mo. The dissimilar welding combination meets both the economic and technical factors and the demands for service. Ferritic/martensitic steel has a lower thermal expansion property, which is better than austenitic steel [44]. However, the failure rate of different weldments increases due to carbon migration from low-alloy to high alloy ferritic steel. The primary cause of dissimilar welding is chromium element, the significant driving force for carbon migration [45–47]. It can even develop from the high-chromium content of filler metal

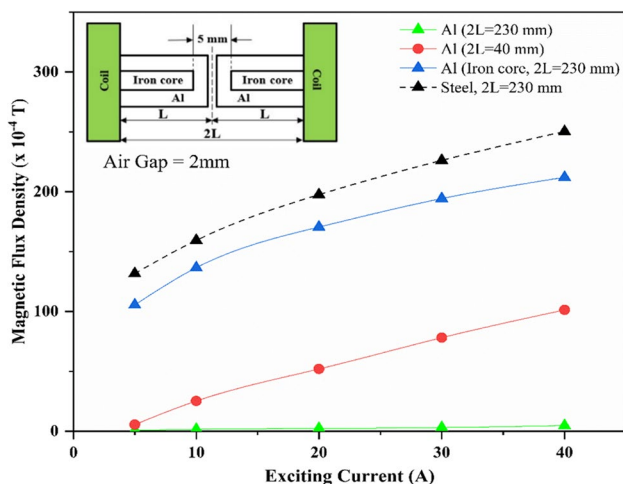


**Fig. 10** Graphical relationship between magnetic flux density (T) and various exciting currents (A) [41]

rods during conventional welding processes. The post-weld heat treatment process reduces carbon migration of the weld interface. It can homogenize the microstructure at the weld interface and improve mechanical properties [48–50]. In MIAB welding, earlier researchers worked on similar welding of T11, T91, and carbon steel tubes. Kumar et al. performed the dissimilar welding of T11 and T91 tubes using MIAB welding. They analyzed their mechanical and microstructural characteristics, showing a good weld quality strength. They also focused on post-weld heat treatment of MIAB-welded dissimilar materials for further study [22]. Dinaharan et al. analyzed the MIAB-welded AISI 409 ferritic steel by radiography test and ensured that they attained better weld quality [51]. Hassel et al. employed MIAB welding to join dissimilar duplex and mild steel. They successfully obtained improved weld properties, and importantly, no notable alteration was observed in the microstructure of the duplex steel [52].

## 4 Weld macrostructure

Earlier researchers reported that the MIAB welding method changed the base metal (BM) microstructure, resulting in the development of a weld zone (WZ) and a thermo-mechanically affected zone (TMAZ) [20, 22, 53]. The welded area, known as the WZ, experiences a lot of plastic deformation and heat. The zone adjacent to WZ is TMAZ, which is subjected to thermal and mechanical deformations. This is mainly happening due to the forging action on the tube material. TMAZ has higher hardness than BM and has higher ductility and tensile strength properties. Microstructural variations in different zones have a significant impact on the post-weld properties of the joint. As a result, researchers must assess the microstructure of the MIAB-welded joint. MIAB-welded joints have different zones, shown in Figure 11a [22]. Figure 11b shows the MIAB-welded dissimilar joints of T11 and T91.

### 4.1 Weld zone

During the MIAB welding, the material coalesces with the other end by forging and forms a weld zone (WZ). There is tremendous heat in the WZ region, creating a plastic deformation that promotes fine grains in the microstructure. A typical microstructure of the MIAB-welded joint is shown in Figure 12 [22]. Figure 12a and b show the MIAB-welded dissimilar joints of the T11 and T91 microstructure. The upset pressure during weld formation influenced the microstructural phase transition at the weld interface. The dislocation density increases by applying the upset pressure, and the dislocation act at the nucleating site. The hardness value of the WZ region is very high compared to the other areas



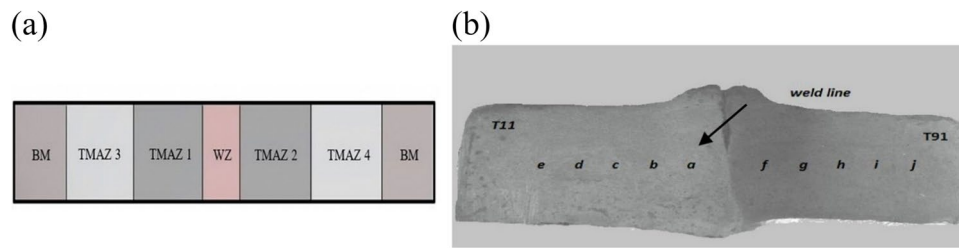
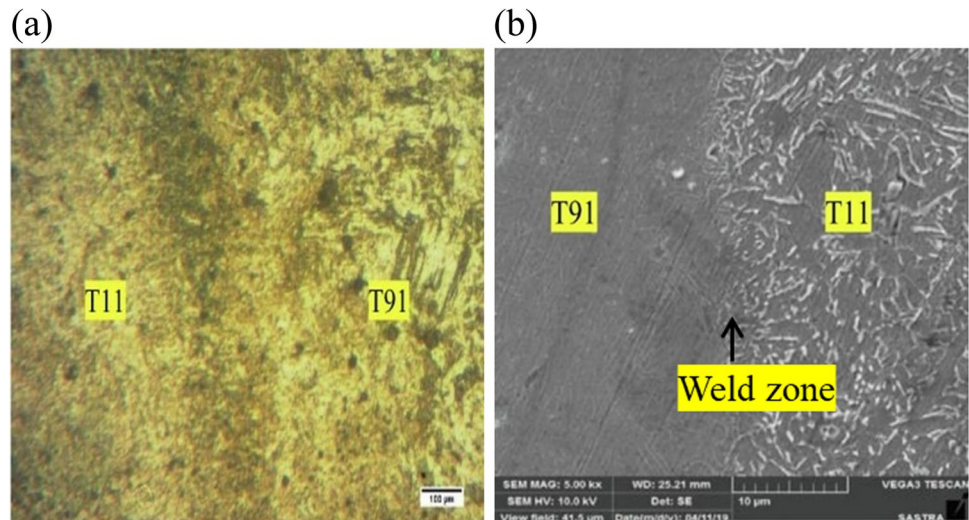


**Fig. 11** **a** Different regions of MIAB-welded joints (BM—base metal, TMAZ—thermo-mechanically affected zone, and WZ—welded zone) [22]. **b** Macrostructure of MIAB-welded dissimilar

joints of T11 and T91 (region a and b—TMAZ 1 of T11, region c and d—TMAZ 2 of T11, region e—BM of T11, region f and g—TMAZ 3 of T91, region h and i—TMAZ 4 of T91, region j—BM of T91 [22])

**Fig. 12** **a** Microstructure of MIAB-welded dissimilar joints of T11 and T91 [22]. **b** MIAB-welded dissimilar joints using SEM analysis [22]



because of the fine-grained microstructure, and the region serves as a nucleation site. R. S. Vidyarthi welded the AISI 409 FSS using multipass tungsten inert gas welding (M-TIG) and activating flux tungsten inert gas welding (A-TIG) and obtained a lower hardness value in the WZ of M-TIG than A-TIG welding [54]. Krishnan et al. experimented with AISI 409 ferritic stainless steel (FSS) using MIAB welding. They found that the weld region is deformed and attained the fine-grained microstructure affected by the compressive force during the upsetting and heat energy of arc [51].

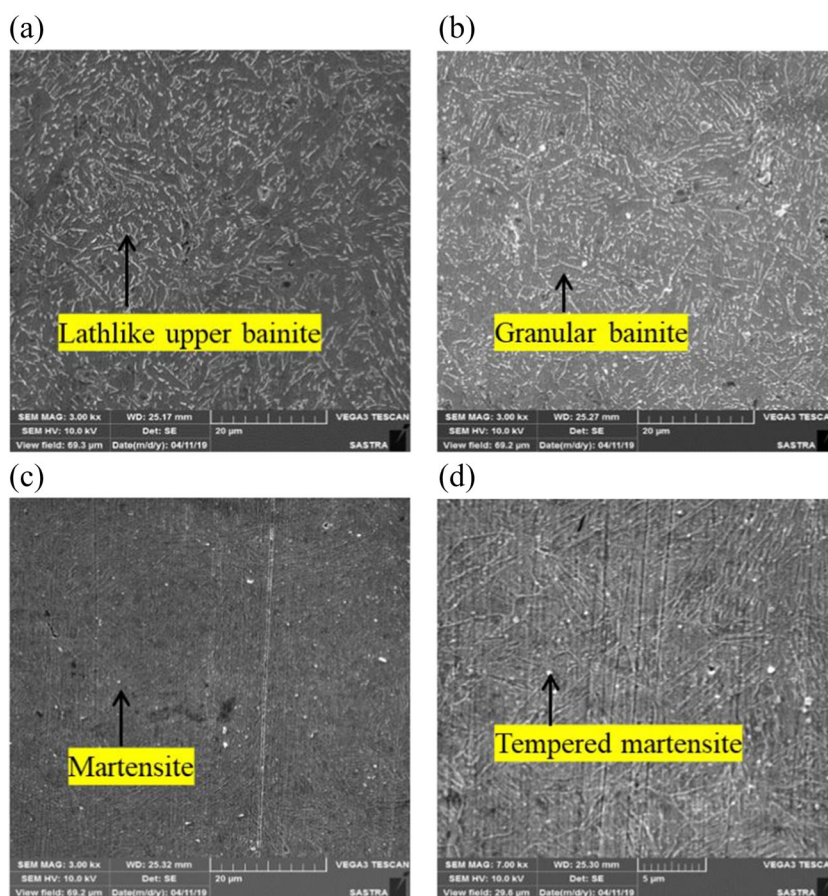
## 4.2 Thermo-mechanically affected zone

Figure 11a shows the TMAZ 1 and TMAZ 2 region occurs nearer to the WZ, which is susceptible to mechanical and thermal deformations. Recrystallization did not happen in this zone due to inadequate deformation strain. Because of inadequate deformation and heat exposure, the grain size in the TMAZ is coarser than the weld area. All welded samples have different TMAZ regions. However, the

microstructure near the weld interface changes depending on the heat applied. The TMAZ 1 obtains lower deformation than the WZ region because of joint forms at the weld interface. Figure 13 shows the different TMAZ regions of MIAB-welded dissimilar T11 and T91 joints [22]. TMAZ regions have higher hardness values, tensile strength, and ductile properties than base metal regions.

The weld interface is surrounded by discrete TMAZs because of the high amperage, high-speed arc rotation, and large temperature gradients generated along the weld line. According to Figure 11a, TMAZ 3 and TMAZ 4 are the areas where the weld thermal cycle has the least impact on the microstructure, acting as the substrate to start the solidification process before moving towards the centre weld line. Due to the temperature effect, at areas far from the weld interface, the TMAZ 3 and TMAZ 4 microstructure differs from that of the TMAZ 1 and TMAZ 2. The low temperature in the TMAZ 3 and TMAZ 4 zone increases grain size during welding because the grains recover, recrystallize, and expand significantly.

**Fig. 13** **a** TMAZ 1 region of T11 [22]; **b** TMAZ 2 region of T11 [22]; **c** TMAZ 1 region of T91 [22]; **d** TMAZ 2 region of T91 [22]



## 5 Mechanical properties of MIAB-welded joint

### 5.1 Hardness

The microstructural variations in the TMAZ region that occurred during MIAB welding of T11 steel tubes were investigated by Sivasankari et al. They noticed that the base metal's hardness of the WZ increased due to the bainitic transition, which also indicated better weld tensile strength and ductility. In all three instances, the TMAZ is inferior to the hardness measured in the weld region, and very narrow TMAZs in the range of 1 mm are achieved in the welded samples [53]. Vignesh et al. experimented with the MIAB welding of T91 tubes, varying the upset current of 900, 1000, and 1100 A. Figure 14 depicts the hardness value of T91 tubes with varying the upset current [55]. The hardness trend strongly suggests that the magnetic field between the tubes produces a large amount of heat when the upset current is high (1100 A). It corresponds to a WZ that cools quickly and hardens to about 600 HV.

Also, the heat created in the region where the tubes join is reduced when the arc current is low (900 A), which typically leads to a lower hardness of 500 HV. As the upset

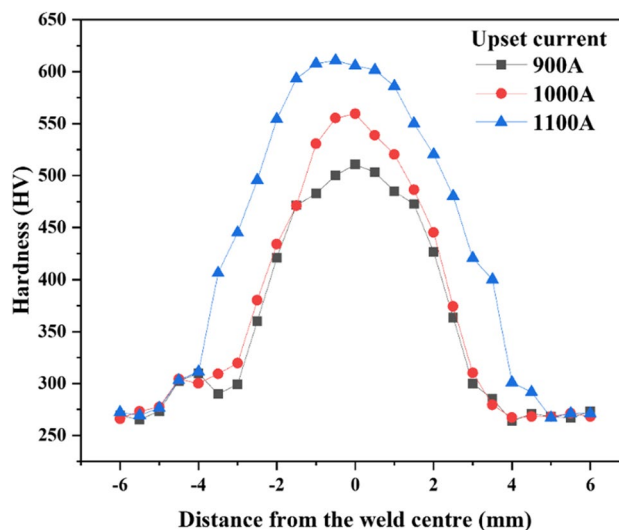


**Fig. 14** Hardness value of T91 tubes with varying upset current [55]

current increased, the hardness of the WZ increased. Ductile cast iron (DCI) and alloy steel, according to Peng et al., have hardness values of about 190 and 200 HV, respectively. The distribution of the microstructure and the change in

hardness were related. In other words, the hardness gradually increased from the TMAZ to the WZ. While the hardness distance from the weld slowly decreased, it suddenly increased to more than 270 HV and reached a maximum of 482 HV. They found that  $\text{Fe}_3\text{Si}_2\text{C}$ , constantly migrating close to TMAZ, was formed in the WZ, causing a sharp increase in the hardness close to the WZ [56].

## 5.2 Tensile strength

Dhiviyasri et al. investigated the differences in the ultimate tensile strength (UTS) of T11 tubes welded by the MIAB welding. They used the PID controller to analyze the welding time and current for the penetration and weld bead, which affects the UTS value [7]. Vignesh et al. successfully welded the T91 tubes and used radiography tests (RT) and computed tomography (CT) images to evaluate the welded joint strength. They observed that the crack formation in the WZ induced the fracture in the weld region [55]. Low-alloy steel pipes 6 mm thick were successfully welded by MIAB welding by Sivasankari et al. The influencing factors are arc rotation current, upset current, and arc rotation time. When the upset current was 800 A and the arc current was 310 A, the maximum tensile strength was 511 MPa. The root bend test revealed no defects from the fracture at the base metal region [53]. Kachinsky et al. performed the MIAB welding on high-strength steels of thick-walled pipes (20 to 320 mm OD with up to 16 mm wall thickness). It is confirmed that the welded joints have high-ductility properties and are equivalent to that base metal strength [57]. High-performance steel with excellent properties is required for various applications, such as energy, construction, and automobile [58]. Vendan et al. imported the data for parametric analysis using machine learning terminologies. The imported data predict the ultimate tensile strength, notch strength ratio, and weld interface hardness values [59]. Using MIAB welding, Peng et al. joined the dissimilar ductile cast iron (DCI) and alloy steel metals. They performed the tensile test and determined that the tensile strength of the weld region was 382.4 MPa. Additionally, the trend values for tensile strength have been increased and decreased. The fracture surface and other

welding defects showed no porosity, showing good mechanical properties of the dissimilarly welded DCI and alloy steel [56]. The different materials that can be welded using the MIAB process are listed in Table 3. The welding current values vary based on the material geometry and properties.

## 6 Welding defects

MIAB welding defects are categorized into two main divisions: inadequate heat and enormous heat. Vignesh et al. experimented with T91 steel tubes of different welding times and varying the upset current. They analyzed the defects using a radiography test (RT) and computed tomography (CT), describing that the samples had more defects and incomplete fusion areas [55]. Defect formation is developed due to the improper optimization of welding parameters such as tube thickness, upset current, and tube gap distances. MIAB welding defects for thin-walled components can be identified as fast and quickly reliable using scanning acoustic microscopy (SAM) with a test duration of around 3 s. For instance, SAM is fast, less expensive than the CT process, and does not risk the operator's health [61].

### 6.1 Defects due to excessive heat

When the arc rotation current increases beyond the optimal value prescribed for the material, it causes excessive heating at joining surfaces, which causes the expulsion of molten metal on the outer surface of the joints in the form of slag, leading to reduced penetration. Excessive melting was caused due to increased arc rotation current, was found to be independent of the time, and increased the energy consumption of the process. To set this arc rotation current to an optimal value, a Proportional-Integral-Derivative (PID) controller was designed by Dhiviyashri et al., which can be auto-tuned based on the feedback obtained [7]. Figure 15 shows the MIAB-welded T11 joint with excessive metal expulsion, leading to material wastage and low weld quality. Due to the extreme running time of arc rotation, excessive material heating occurs while running to an optimum

**Table 3** Various materials being welded by MIAB welding technique

S. no.	Materials	Wall thickness(mm)	Arc initiation current ( $I_1$ )	Arc rotation current ( $I_2$ )	Upset current ( $I_3$ )	Ultimate tensile strength (MPa)	References
1.	Alloy steel	6.6–7	280	200	1100	506	[7]
2.	Carbon steel	4.5	330	310	1000	471 ± 23.6	[20]
3.	Alloy steel	6	310	290	1000	541	[53]
4.	Carbon steel	4.5	300	280	1200	458	[21]
5.	Carbon steel	5–6	330	310	1100	450	[14]
6.	Alloy steel	6–7	280	200	1100	506	[60]



**Fig. 15** MIAB-welded T11 joint with excessive metal expulsion [7]

with all current inputs. Arc rotation time plays a vital role in creating a stable arc that heats the tube edges and exceeds the optimal time, resulting from excessive melting. The arc rotation time varies depending on the material properties and its geometry.

## 6.2 Defects due to inadequate heat input

The main reason for cracks in MIAB-welded joints was the inadequate heat input supplied during the welding. Iordachescu et al. provide a longitudinal magnetic system coupled with peripheral solenoids for better magnetic flux concentration. It is found that the amount of welding current lesser than the required level causes improper heating and reduced deformation, which in turn causes the formation of weaker weld joints. The authors further stated that magnetic flux density significantly impacts producing better arc rotation and providing the required heating duration [8]. The defects of inadequate heat input are improved by proper arc rotation time, which significantly improves the penetration and tends to increase the tensile strength. This can be varied depending on the material geometry and its properties.

## 7 Applications of MIAB welding technique

In power, oil, and gas sectors, the MIAB welding method is widely used, replacing other welding processes like friction, flash, butt, and resistance welding [24]. The automobile industry increases Al alloy usage for better heat reduction and lowers vehicle weight. MIAB welding offers many advantages in joining Al alloys for automobile industries. The most important thing is to join Al alloys with steel and draw worldwide attention due to their high load-bearing ability. Welding the rear axle of the Ford Fiesta car provides an instance where MIAB welding is employed on a safety-critical joint. Since 1977, the flanged spindles have been securely welded to a double-cranked cross tube using MIAB welding. The joint dimensions are 60 mm OD and 2.5 mm thickness, necessitating an arc heating duration of approximately 2.5 s and a direct current of around 600 A. Three automatic double-ended machines simultaneously execute both welds. MIAB was selected instead of friction welding due to the precise alignment required between the spindle flanges and the cranked tube. Another smaller application involves welding an end cap to a low-carbon steel tube with dimensions of 22 mm OD and 1 mm wall thickness. This welding process is utilized for hatchback door gas struts. A fully automatic machine, loaded in batches, completes the welding with a cycle time of 6 s, using an arc time of less than 1 s [17]. Several researchers attempted a similar joining of alloys in MIAB welding and its characterization with varying input parameters. The titanium (Ti) alloy is a lightweight metal with more strength than steel, demonstrating a high corrosion resistance. Many researchers are still attempting joints on titanium alloys with other alloys like Al and Cu. However, MIAB welding has already started joining Ti alloys, and its characterization works in the industry. Successful welds are made on different joining of alloys like Al and Cu joints. Table 4 shows MIAB welding applications with their respective dimensions. Moreover, it is a single-step process that reduces working time and improves productivity.

**Table 4** Applications of MIAB welding with their respective dimensions

S. no.	Description	Outer diameter	Wall thickness	References
1.	A welded joint of the tube	219 mm	8 mm	[8]
2.	Cardan shaft	75.2 mm	2.1 mm	
3.	Shock absorber	53 mm	1.8 mm	
4.	Pneumatic spring	53 mm	1.8 mm	

## 8 Conclusions

The research on MIAB welding has identified that it does not require edge preparation, skilled labour, filler material, and shielding gas. The tubes are not rotating and can be joined by upsetting through the linear movement of the moving tube material. The non-rotating parts of the welded tubes produce minimum friction and increase machine life. Shorter weld times, uniform heating, non-appearance of pores, and high performance in the mass manufacturing industries are the main benefits of MIAB welding. MIAB weld process runs through the primary process parameters like magnetic coil current, coil position, and welding current, which govern the arc speed. To achieve better surface integrity of tubes, the parameters must be maintained to obtain excellent weldment. The following are the significant findings that may be derived from this review article to improve weld strength:

- (1) The welding current and time durations are kept within the required range based on the material properties, tube thickness, geometry, and gap size. However, suppose these current and duration values are maintained. In that case, the weld created may exhibit changes due to weld surface imperfections or differences in upset pressure and rate of application of pressure, magnetic properties, and gap size.
- (2) Maintaining the air gap distance of the tubes at 1.5 to 2 mm is essential. If the gap is over 2 mm, the arc will not produce a long run, leading to no weld.
- (3) Arc rotation evolves after the arc initiation, which involves obtaining a defect-free weld.
- (4) Arc speed is also a significant factor that can be increased by higher EMF, forming a better weldment of the tubes. The higher EMF has been achieved by maintaining a tube gap distance, coil position, and coil excitation.
- (5) Increasing excitation current in the coil increases the value of magnetic flux density in the tube gap distance.
- (6) The upsetting phase is essential for maintaining a high current above 800 A for 0.3 seconds before forging to obtain a better weld quality. Below 800 A of upset current produces a deformation zone at the weld interface.

## 9 Future outlook

- (1) The cylindrical components can be welded within a short period. But there is limited research on the dissimilar joining of tube material, and it will explore the benefits of this MIAB welding technique in automobile and boiler components.

- (2) The optimum values of welding input parameters are not yet identified for the ferrous materials. It should be tried using optimization techniques like response surface methodology (RSM) and ANN, to simulate the response results properly.
- (3) Post-weld heat treatment should be carried out, and the results should be compared between MIAB-welded and post-weld heat-treated samples. Researchers will explore the post-weld heat treatment of MIAB-welded joints in the future, enhancing the weld quality.
- (4) Researchers must explore the different thicknesses of steel tube material with varying process parameters of MIAB welding.

**Acknowledgements** The author would like to thank the SASTRA Deemed to be University for their assistance.

**Author contributions** S. Santhosh Kumar: investigation, methodology, resources, writing—original draft

S. Ramesh Kumar: conceptualization, formal analysis, supervision, validation, writing—review and editing

**Funding** This work was supported financially by the “Department of Science and Technology, Government of India, through SERB under the ECR scheme”, with the grant number ECR/2017/003021.

## Declarations

**Competing interests** The authors declare no competing interests.

## References

1. Yapp D, Blackman SA (2004) Recent developments in high productivity pipeline welding. *J Brazilian Soc Mech Sci Eng* 26:89–97. <https://doi.org/10.1590/S1678-58782004000100015>
2. Komizo Y-I (2008) Overview of recent welding technology relating to pipeline construction. *Trans JWRI* 37:1–5
3. Vendan SA, Manoharan S, Buvanashakaran G, Nagamani C (2009) Development of a MIAB welding module and experimental analysis of rotational behavior of arc-simulation of electromagnetic force distribution during MIAB welding of steel pipes using finite element analysis. *Int J Adv Manuf Technol* 43:1144–1156. <https://doi.org/10.1007/s00170-008-1793-x>
4. Phillips DH (2008) Magnetically impelled arc butt (MIAB) welding of chromium-plated steel tubular components utilizing arc voltage monitoring techniques. The Ohio State University
5. Chaturvedi M, Subbiah AV, Tharwan MY, et al (2022) Welding of low carbon steel tubes using magnetically impelled arc butt welding: experimental investigation and characterization. *Metals (Basel)* 12:1965. <https://doi.org/10.3390/met12111965>
6. Vendan SA, Manoharan S, Buvanashakaran G, Nagamani C (2011) Magnetically impelled arc butt welding of alloy steel tubes in boilers - establishment of parameter window. *Mechatronics* 21:30–37. <https://doi.org/10.1016/j.mechatronics.2010.08.001>
7. Dhivyasri G, Rahul SG, Kavitha P et al (2018) Dynamic control of welding current and welding time to investigate ultimate tensile

- strength of miab welded T11 tubes. *J Manuf Process* 32:564–581. <https://doi.org/10.1016/j.jmapro.2018.03.031>
8. Kachinsky VS, Krivenko VG, Ignatenko VY (2002) Magnetically impelled arc butt welding of hollow and solid parts. *Weld World* 46:49–56. <https://doi.org/10.1007/BF03263390>
  9. Taneko A, Arakida F, Takagi K (1987) Analysis of arc rotation velocity in magnetically impelled arc butt welding. *Weld Int* 1:247–253. <https://doi.org/10.1080/09507118709452125>
  10. Sato T, Katayama J, Ioka S, Otani M (1991) An experimental study of rotational behaviour of the arc during magnetically impelled arc butt welding. *Weld Int* 5:5–10. <https://doi.org/10.1080/09507119109447814>
  11. Iordachescu D, Iordachescu M, Georgescu B et al (2010) Technological windows for MIAB welding of tubes featuring original longitudinal magnetization system with peripheral solenoids. *J Mater Process Technol* 210:951–960. <https://doi.org/10.1016/j.jmatprotec.2010.02.007>
  12. Kuchuk-Yatsenko SI (1988) Control of the arc moving in a narrow gap under the effect of a magnetic field in press welding of pipes. *Weld Int* 2:965–968. <https://doi.org/10.1080/09507118809447587>
  13. Kim JW, Choi DH (2003) A study on the numerical analysis of magnetic flux density by a solenoid for magnetically impelled arc butt welding. *Proc Inst Mech Eng Part B J Eng Manuf* 217:1401–1407. <https://doi.org/10.1243/095440503322617171>
  14. Arungalai Vendan S, Mundla SR, Buvanashakaran G (2012) Feasibility of magnetically impelled arc butt (MIAB) welding of high-thickness tubes for pressure parts. *Mater Manuf Process* 27:573–579. <https://doi.org/10.1080/10426914.2011.585488>
  15. Sk AK, Khan N (2018) An experimental investigation of magnetically impelled arc butt welding of pipes: a review. *Int J Curr Eng Technol* 8:535–540. <https://doi.org/10.14741/ijcet/v.8.3.8>
  16. Panda BN, Vendan SA, Garg A (2017) Experimental- and numerical-based studies for magnetically impelled arc butt welding of T11 chromium alloy tubes. *Int J Adv Manuf Technol* 88:3499–3506. <https://doi.org/10.1007/s00170-016-9057-7>
  17. Westgate SA, Edson DA (1986) The miab welding of tubular sections for mass production industries. *SAE Tech Pap*. <https://doi.org/10.4271/860582>
  18. Arungalai Vendan S, Thangadurai V, Vasudevan A, Senthil Kumar A (2014) Investigations on temperature distribution during revolutionary and zigzag movement of arc in magnetically impelled arc butt welding of tubes. *Int J Appl Electromagn Mech* 46:155–163. <https://doi.org/10.3233/JAE-141768>
  19. Patel VC, Patel PDH (2018) Microstructure analyses of magnetic impaled arc beam (miab) welding specimen. *Int J Adv Eng Res Dev* 05:677–682
  20. Sivasankari R, Balusamy V, Venkateswaran PR et al (2018) Light band zone formation and its influence on properties of magnetically impelled arc butt (MIAB) welded carbon steel tubes. *Trans Indian Inst Met* 71:351–360. <https://doi.org/10.1007/s12666-017-1185-8>
  21. Sivasankari R, Balusamy V, Buvanashakaran G (2014) Effect of upset current in magnetically impelled arc butt (MIAB) welding of carbon steel tubes. *Appl Mech Mater* 592–594:240–244. <https://doi.org/10.4028/www.scientific.net/AMM.592-594.240>
  22. Ramesh Kumar S, Ravishankar B, Vijay M (2020) Prediction and analysis of magnetically impelled arc butt welded dissimilar metal. *Mater Today Proc* 27:2037–2041. <https://doi.org/10.1016/j.matpr.2019.09.054>
  23. Suresh Isravel R, Saravanan S, Venkateswaran PR (2020) Exploration of magnetically impelled arc butt welded SA210GrA tubes for boiler applications. *Mater Today Proc* 21:123–126. <https://doi.org/10.1016/j.matpr.2019.05.374>
  24. Norrish J, Cuiuri D, Hossain M (2005) Modelling and simulation of the magnetically impelled arc butt (MIAB) process for transmission pipeline applications. In: *Int Pipeline Integr Conf Aust WITA*. Weld Technol Insitute
  25. Kachinsky VS, Kuchuk-Yatsenko SI, Koval MP, Goncharenko EI (2016) Technology and equipment for press magnetically-impelled arc welding of position joints of small-diameter pipes in site and stationary conditions. *Pat Weld J* 2016:29–34. <https://doi.org/10.15407/tpwj2016.06.05>
  26. Vendan SA, Manoharan S, Buvanashakaran G, Nagamani C (2009) Simulation of magnetic flux distribution for magnetically impelled arc butt welding of steel tubes. *Multidiscip Model Mater Struct* 5:229–234. <https://doi.org/10.1163/157361109789017096>
  27. Vendan SA, Manoharan S, Buvanashakaran G, Nagamani C (2008) Magnetic flux distribution modelling of magnetically-impelled arc butt-welding of steel tubes using finite-element analysis. *Proc Inst Mech Eng Part C J Mech Eng Sci* 222:1783–1790. <https://doi.org/10.1243/09544062JMES1025>
  28. Edition F (2014) *Physical metallurgy*. Elsevier
  29. Kou S (2002) *Welding Metallurgy*. Wiley
  30. Meazza M, Rios R (2016) Merging transition-metal activation and aminocatalysis. *Synthesis (Stuttg)* 48:960–973. <https://doi.org/10.1055/s-0035-1561328>
  31. Amandeep SS, Er. Sandeep KS (2017) Refurbishment of ASTM A213 T-11 steel boiler tubes. *Int J Latest Trends Eng Technol pp* 254–257
  32. Norrish J (2006) *Advanced welding processes*. Woodhead Publishing Limited
  33. Nandakumar N, Nandhini P (2015) Investigating the characterization of magnetically impelled arc butt welding. *Int J Sci Eng Technol Res* 4:3747–3750
  34. Vendan SA, Manoharan S, Nagamani C (2012) MIAB welding of alloy steel tubes in pressure parts: metallurgical characterization and non destructive testing. *J Manuf Process* 14:82–88. <https://doi.org/10.1016/j.jmapro.2011.09.006>
  35. Higgins R (1999) *Engineering metallurgy: applied physical metallurgy*. Edward Arnold 1999:560
  36. Islam T, Rashed HMMA (2019) Classification and application of plain carbon steels. In: *Reference module in materials science and materials engineering*. Elsevier
  37. Nikolay A Belov DGE and AAA (2018) *Multicomponent phase diagrams*. Elsevier
  38. Sankaran KK, Mishra RS (2017) *Metallurgy and design of alloys with hierarchical microstructures*. Elsevier
  39. Mathers G (2002) *The Welding of Aluminium and its Alloys*, 236
  40. Löveborn D, Larsson JK, Persson KA (2017) Weldability of aluminium alloys for automotive applications. *Phys Procedia* 89:89–99. <https://doi.org/10.1016/j.phpro.2017.08.011>
  41. Mori S, Yasuda K (1989) Magnetically impelled arc butt welding of aluminium pipes. *Weld Int* 3:941–946. <https://doi.org/10.1080/09507118909449057>
  42. Sirohi S, Gupta A, Pandey C et al (2022) Investigation of the microstructure and mechanical properties of the laser welded joint of P22 and P91 steel. *Opt Laser Technol* 147:107610. <https://doi.org/10.1016/j.optlastec.2021.107610>
  43. Sunilkumar D, Muthukumaran S, Vasudevan M, Reddy GM (2021) Microstructure and mechanical properties relationship of friction stir- and A-GTA-welded 9Cr-1Mo to 2.25Cr-1Mo Steel. *J Mater Eng Perform* 30:1221–1233. <https://doi.org/10.1007/s11665-020-05426-0>
  44. Ennis PJ (2014) Ferritic and martensitic steels for power plants. In: *Structural Alloys for Power Plants*. Woodhead Publishing, pp 188–220
  45. Wang Q, Shao C, Cui H et al (2022) Effect of carbon migration on interface fatigue crack growth behavior in 9Cr/CrMoV dissimilar welded joint. *Acta Metall Sin (English Lett)* 35:714–726. <https://doi.org/10.1007/s40195-021-01322-1>

46. Sirohi S, Pandey C, Goyal A (2020) Role of heat-treatment and filler on structure-property relationship of dissimilar welded joint of P22 and F69 steel. *Fusion Eng Des* 159:111935. <https://doi.org/10.1016/j.fusengdes.2020.111935>
47. Thakare JG, Pandey C, Mahapatra MM, Mulik RS (2019) An assessment for mechanical and microstructure behavior of dissimilar material welded joint between nuclear grade martensitic P91 and austenitic SS304 L steel. *J Manuf Process* 48:249–259. <https://doi.org/10.1016/j.jmapro.2019.10.002>
48. Adhithan B, Pandey C (2021) Study on effect of grain refinement of P92 steel base plate on mechanical and microstructural features of the welded joint. *Int J Press Vessel Pip* 192:104426. <https://doi.org/10.1016/j.ijpvp.2021.104426>
49. Sirohi S, Taraphdar PK, Dak G et al (2021) Study on evaluation of through-thickness residual stresses and microstructure-mechanical property relation for dissimilar welded joint of modified 9Cr–1Mo and SS304H steel. *Int J Press Vessel Pip* 194:104557. <https://doi.org/10.1016/j.ijpvp.2021.104557>
50. Dak G, Pandey C (2021) Experimental investigation on microstructure, mechanical properties, and residual stresses of dissimilar welded joint of martensitic P92 and AISI 304L austenitic stainless steel. *Int J Press Vessel Pip* 194:104536. <https://doi.org/10.1016/j.ijpvp.2021.104536>
51. Dinaharan I, Muthu Krishnan T, Palanivel R (2022) An assessment of microstructure and tensile behavior of magnetically impelled arc butt welded AISI 409 ferritic stainless steel tubes. *J Mater Eng Perform*. 31(10):7808–7819. <https://doi.org/10.1007/s11665-022-06806-4>
52. Hassel T, Maier HJ, Alkhimenko A et al (2022) Investigation of the mechanical properties and corrosion behaviour of hybrid L 80 type 1 and duplex steel joints produced by magnetically impelled arc butt welding. *J Adv Join Process* 5:100109. <https://doi.org/10.1016/j.jajp.2022.100109>
53. Sivasankari R, Balusamy V, Venkateswaran PR et al (2015) Characterization of magnetically impelled arc butt welded T11 tubes for high pressure applications. *Def Technol* 11:244–254. <https://doi.org/10.1016/j.dt.2015.03.005>
54. Vidyarthi RS, Dwivedi DK, Vasudevan M (2017) Influence of M-TIG and A-TIG welding process on microstructure and mechanical behavior of 409 ferritic stainless steel. *J Mater Eng Perform* 26:1391–1403. <https://doi.org/10.1007/s11665-017-2538-5>
55. Vignesh S, Dinesh Babu P, Prasanna Venkatesh V et al (2017) Experimental investigations on magnetically impelled arc butt welded T91 steel tubes. *Trans Indian Inst Met* 70:741–748. <https://doi.org/10.1007/s12666-017-1086-x>
56. Peng M, Liu H, Xuan Y et al (2021) Evaluation of the microstructural and mechanical properties of ductile cast iron and alloy steel dissimilar materials welded by magnetically impelled arc butt. *J Mater Res Technol* 15:4623–4635. <https://doi.org/10.1016/j.jmrt.2021.10.059>
57. Kachinsky VS, Kuchuk-Yatsenko SI (2017) Joint formation in magnetically-impelled arc butt welding of thick-walled pipes from high-strength steels. *Pat Weld J* 2017:39–45. <https://doi.org/10.15407/tpwj2017.08.06>
58. Tapas KR, Basudev B, Chiradeep Ghosh SKA (2018) Advanced high strength steel. Springer Singapore, Singapore
59. Vendan SA, Kamal R, Karan A, et al (2020) Supervised machine learning in magnetically impelled arc butt welding (MIAB). In: *Engineering Applications of Computational Methods*. Springer Singapore, pp 1–56
60. Arungalai Vendan S, Manoharan S, Buvanashakaran G, Nagamani C (2012) Strength assessment using destructive testing on MIAB welded alloy steel tubes and subsequent techno-economical evaluation. *J Manuf Process* 14:328–335. <https://doi.org/10.1016/j.jmapro.2011.12.001>
61. Kustroń P, Piwowarczyk T, Korzeniowski M et al (2020) The detectability of welding defects in miab welded thin-walled tubular components by immersion ultrasonic technique. *J Nondestruct Eval* 39:42. <https://doi.org/10.1007/s10921-020-00684-3>

**Publisher's note** Springer Nature remains neutral with regard to jurisdictional claims in published maps and institutional affiliations.

Springer Nature or its licensor (e.g. a society or other partner) holds exclusive rights to this article under a publishing agreement with the author(s) or other rightsholder(s); author self-archiving of the accepted manuscript version of this article is solely governed by the terms of such publishing agreement and applicable law.